Radiation Physics and Chemistry 209 (2023) 110946

Contents lists available at ScienceDirect

Radiation Physics and Chemistry

journal homepage: www.elsevier.com/locate/radphyschem

A fast algorithm for real-time monitoring of artificial radioisotopes in presence of variable natural radioactivity

A. Cerezo *, E. Prieto, I. Reichardt, R. Casanovas, M. Salvadó

Unitat de Física Mèdica, Facultat de Medicina i Ciències de la Salut, Universitat Rovira i Virgili, Sant Llorenç 21, ES-43201, Reus, Tarragona, Spain

ARTICLE INFO

Handling Editor: Chris Chantler

Keywords:
Scintillation gamma-ray spectrometry
$LaBr_3$(Ce)
SrI_2(Eu)
Early warning
Natural isotope
Environmental surveillance network

ABSTRACT

We present an agile, hardware independent analysis methodology based on the spectral windows technique to detect and quantify the environmental activity concentration of artificial isotopes of interest. The method removes counts from Compton scattering, peak overlapping, intrinsic background and other unconsidered contributions to the spectral region where photopeaks from artificial elements are expected. Taking into account the varying concentration of ^{214}Bi, ^{214}Pb, and ^{212}Pb, we compute the activity concentration of the artificial isotopes (when detectable), or a variable Minimum Detectable Activity Concentration (MDAC). This allows to set statistically robust early-warning levels. In the scenario with the lowest concentration of natural occurring isotopes, and for 10-min integration time, we achieve a MDAC of 5.4/4.1/3.9 (Bq/m^3) for ^{131}I/^{137}Cs/^{60}Co using a $LaBr_3$(Ce) detector; and 4.2/2.8/2.7 (Bq/m^3) for ^{131}I/^{137}Cs/^{60}Co with a SrI_2(Eu) detector.

1. Introduction

In Catalonia (North-East Spain) there are three nuclear power plants in operation housed in two nuclear power plants named Ascó and Vandellòs. For that reason, a continuous surveillance of the artificial isotopes present in the environment is a priority for the Catalan Government, which in the last years has been promoting upgrades in the Radiological Surveillance Network of Catalonia (XVRAC, Xarxa de Vigilància Radiològica Ambiental de Catalunya). The Medical Physics Unit of Universitat Rovira i Virgili has participated in the expansion and evolution of the Radiological Surveillance Network of Catalonia since 2006. We have contributed to the Network designing and testing different types of radiation monitors and developing automatic real time analysis methods for the establishment of early warning alarms. The Network currently has 38 gamma spectrometry radiation monitors with scintillation detectors that acquire spectra every 10 min.

The monitors of the Catalan Network are grouped into four structures with spectrometric measurement capacity: the first one has twenty-four direct monitors without shielding (with 1″ × 1″ or 2″ × 2″ $LaBr_3$(Ce) detectors, 3″ × 3″ NaI(Tl) detectors and 2″ × 2″ SrI_2(Eu) detectors), the second structure has ten monitors for aerosol surveillance using a particulate filter (RARM-F) (Casanovas et al., 2014a) with 2″ × 2″ $LaBr_3$(Ce) and SrI_2(Eu) detectors, the third structure has two monitors with direct measurement using two shielded detectors (RARM-D2) (Casanovas et al., 2014b), with either NaI(Tl) or $LaBr_3$(Ce) detectors, and the fourth structure has two NaI(Tl) water monitors (Casanovas et al., 2013) for the surveillance of the water from Ebre River that were also tested with $LaBr_3$(Ce) detectors (Prieto et al., 2018a).

When monitoring artificial isotopes in the environment with on-field gamma spectrometry detectors, it is well known that ^{222}Rn gamma descendants (namely ^{214}Pb and ^{214}Bi) and elements of the ^{232}Th decay chain (^{208}Tl, ^{228}Ac, ^{212}Pb or ^{212}Bi) will be detected. Other known radionuclides, like ^{40}K, are also detectable. However, the ^{212}Pb, ^{214}Pb and ^{214}Bi gamma-ray emission lines are of particular interest. This is because these lines vary their intensity with the variations of radon emanation, which is directly related to meteorological conditions (Casanovas et al., 2011) (Márquez et al., 2017) (Vallés et al., 2009). Therefore, while e.g., ^{40}K emission is almost constant for a given monitoring site (Vallés et al., 2009) (Baeza et al., 2016) (Hötzl and Winkler, 1987), the emission from radon descendants can vary by a large factor. As we will discuss below, this varying emission can be confounded with the appearance of an artificial source of radioactivity, and thus, can generate a false positive detection, and ultimately limit the ability to determine an alert threshold for the detection of artificial radionuclides.

Analytic methods used to determine the activity concentration of artificial isotopes of interest in environmental spectra must consider natural contributions. Some methods have been developed to obtain the maximum information from gamma spectra and, thus, are useful to

* Corresponding author.
E-mail address: agustin.cerezo@urv.cat (A. Cerezo).

https://doi.org/10.1016/j.radphyschem.2023.110946
Received 2 August 2022; Received in revised form 11 March 2023; Accepted 27 March 2023
Available online 11 April 2023

establish early warning alarms. Among these methods are the calculation of the ambient dose equivalent H*(10) from gamma-ray spectra (Casanovas et al., 2016), spectral regions analysis methods (Korbech and Nielsen, 1992) (Cresswell et al., 2006) (International Atomic Energy Agency, 1999) and full spectrum analysis methods (Hendriks et al., 2001) (Androulakaki et al., 2016).

Given the variety of monitors, detector crystal types and dimensions of the different Network stations, we developed a method based on spectral regions or ROIs (Regions of Interest) to analyse automatically and in real time the great quantity of spectra registered (Prieto et al., 2018b). This method was validated and tested previously, however it required of a long and laborious procedure to be implemented in each monitor on field as it was necessary to perform in situ measurements with known test sources at different distances from the detector.

In this study, we present an evolution of the ROIs method to efficient and constantly monitor the activity concentration of artificial radioisotopes. In this new approach, we obtain the activity concentration of artificial radionuclides by means of an algorithm that considers contributions from frequent natural gamma emitters that are present in certain ROIs. These contributions arise from photopeaks of natural radioisotopes, Compton scattering, detector background or from other unconsidered sources. Ultimately, we assume that the ROI where an artificial photopeak is expected receives a linear combination of contributions from the varying ^{214}Bi, ^{214}Pb, and ^{212}Pb, plus a constant contribution. The parameters of the method are the proportionality coefficients of each contribution. In this regard, our method is a form of full spectrum analysis where variations are mostly expected from the three above-mentioned natural isotopes, and all other contributions are aggregated in the constant term.

The new method permits us to obtain the algorithm parameters in a much simpler way. We make use of the environmental background where the detector is placed instead of preparing a set of in situ measurements with point-like sources of natural and artificial radioisotopes at different distances from the detector. We also use spectra obtained in the laboratory to adjust the counts per second (cps) of the artificial isotopes of interest (measured on field) in activity concentration units (Bq/m^3). This procedure is useful to calibrate all the on-field monitors remotely, which makes the process easier, faster, economical, and as accurate as the previous method.

We particularize and test the calculations for $LaBr_3$(Ce) and SrI_2(Eu) detectors to monitor various activity concentrations of ^{137}Cs, ^{131}I and ^{60}Co considering the variations of the Rn and Th descendants ^{212}Pb, ^{214}Pb and ^{214}Bi. Moreover, we develop the full uncertainty propagation that permits the determination of conditions-dependent detection limits, in compliance with the ISO 11929 standard (ISO 11929-1, 2019). The method can be extended to the case where other natural radioisotopes are present and other artificial radioisotopes need to be monitored.

2. Materials

The available equipment to perform this study were a 2″×2″ $LaBr_3$(Ce) detector (BrilLance™380 from Saint-Gobain Crystals®) coupled to a digital multichannel analyser (Digibase from Ortec®) and a 2″×2″ SrI_2(Eu) detector (ScintiClear™ from CapeSym®) also coupled to a digital multichannel analyser (eMorpho from Bridgeport Instruments®). We obtained the experimental data using radioactive sources: a point-like source of ^{137}Cs, a point-like source of ^{60}Co, an encapsulated source of ^{131}I and a hermetically sealed source containing ^{226}Ra in equilibrium with the gamma emitting ^{222}Rn descendants (mainly ^{214}Pb and ^{214}Bi) and ^{224}Ra in equilibrium with the gamma emitting ^{220}Rn descendants (mainly ^{212}Pb). We will refer to the sealed source of ^{226}Ra and ^{224}Ra as the source of natural isotopes.

3. Methods

3.1. Spectra pre-processing

Before the application of any analysis method, each registered spectrum must be stabilized and calibrated in energy, resolution and efficiency to perform activity concentration calculations.

3.1.1. Spectra stabilization

Environmental gamma spectra suffer peak shifting, mainly due to ambient temperature variations. We stabilized spectra automatically using a self-developed software that applies a previously described methodology (Casanovas et al., 2012a). This procedure is also applied to spectra obtained in the laboratory to prevent peak shifting due to possible changes in the temperature.

3.1.2. Energy and resolution calibrations

The energy and resolution calibrations are obtained using sources with main presence of ^{238}U descendants (^{226}Ra, ^{214}Pb, ^{214}Bi …) and other elements detected in the spectrum, like ^{40}K and ^{138}La (see Fig. 1). The natural isotopes source was placed at 40 cm from the detector, obtaining a spectrum showed in Fig. 1, and involving the activity concentrations for ^{214}Bi, ^{214}Pb and ^{212}Pb shown in “Natural” scenario in Fig. 2. The resulting spectrum is used to obtain the resolution and energy calibrations fitting a second order polynomial (Casanovas et al., 2012b):

$$E(C) = a_0 + a_1 \cdot C + a_2 \cdot C^2 \quad (1)$$

$$FWHM(E) = b_0 + b_1 \cdot E + b_2 \cdot E^2 \quad (2)$$

The energy and FWHM(E) calibration curves are presented in Appendix II.

3.1.3. Efficiency calibration

We calibrated the spectra in efficiency to obtain activity concentrations in Bq/m^3. The efficiency calibrations are performed using Monte Carlo simulations with EGS5 code. The isotopes are assumed to be homogeneously distributed in air, forming a cylindrical source of equal height and diameter of 500 m (‘infinite’ source) surrounding the detector. More details about the efficiency calculation are given in a previous study (Casanovas et al., 2014b). The efficiency calibration curves are presented in Appendix II.

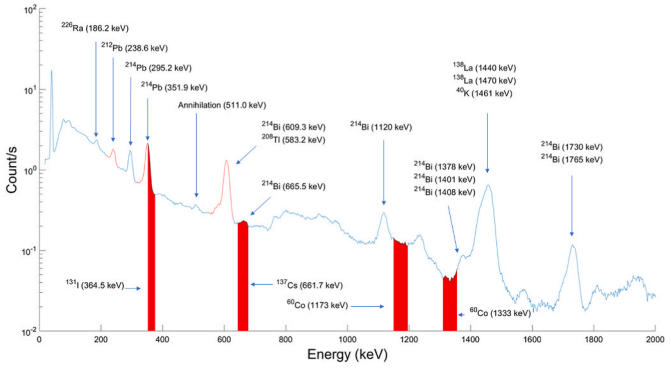

Fig. 1. Environmental spectra obtained with a $LaBr_3$(Ce) detector in laboratory where main natural isotopes present in the environment and ^{138}La emissions at 1440 keV and 1470 keV from the detector self-contamination are identified (blue arrows). These emissions are also used for the energy calibration calculation of $LaBr_3$(Ce) detectors. The red areas mark the ROIs of study for the artificial isotopes ^{131}I, ^{137}Cs and ^{60}Co and the red lines mark the ROIs of study for the natural isotopes ^{212}Pb, ^{214}Pb and ^{214}Bi. Note that this is a spectrum with only presence of natural isotopes, the peak around 665 keV corresponds to the 665.5 keV emission of ^{214}Bi. There is not presence of ^{137}Cs or another artificial isotope.

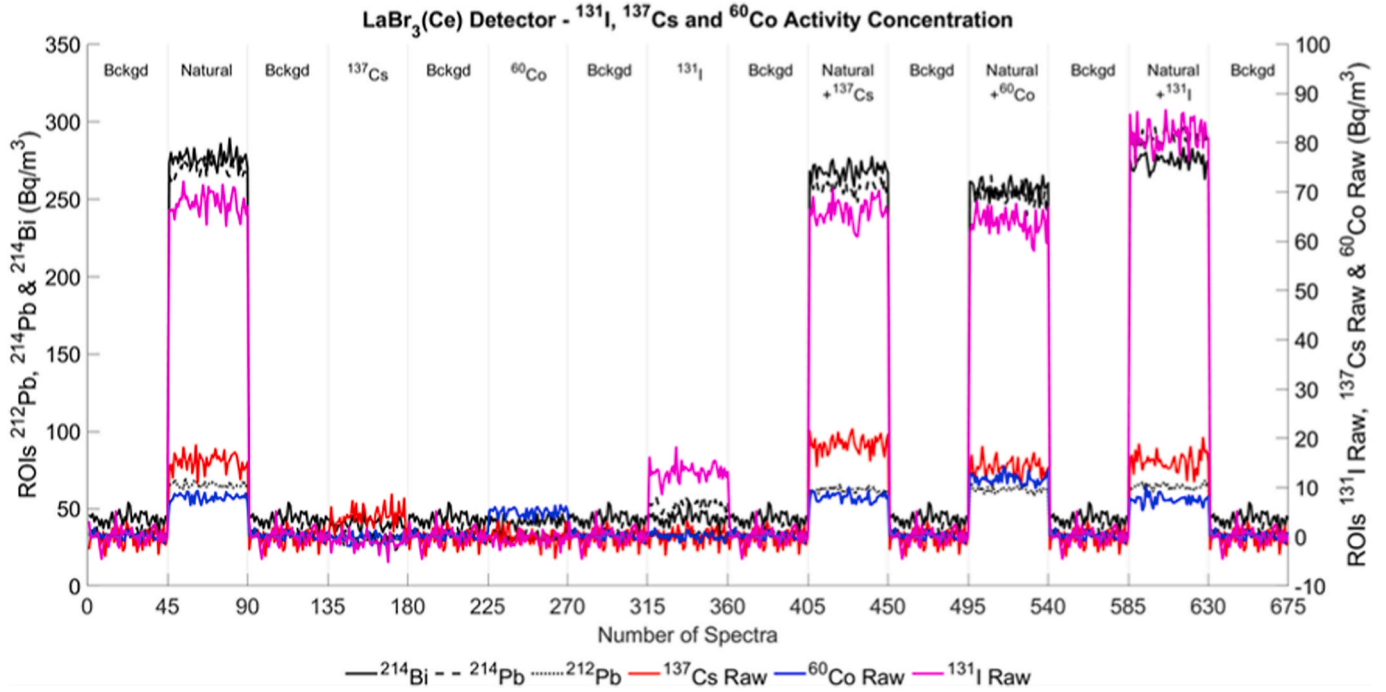

Fig. 2. Raw data for the $LaBr_3$(Ce) detector with scenarios with natural, ^{131}I, ^{137}Cs and ^{60}Co isotopes sources. The measurements are shown from left to right: Background (0–45), the natural source at x = 40 cm (45–90), background (90–135, 180–225 and 270–315), artificial isotope source at x = 100 cm (135–180, 225–270 and 315–360), background (360–450), the combination of the natural source and the artificial isotope at x = 40 and 100 cm (405–450, 495–540 and 585–630) and background (450–495, 540–585 and 630–675).

3.1.4. Regions of Interest width determination

Once the spectra are stabilized and the detectors are calibrated in energy and resolution, we can define a Region of Interest (ROI) as the energy range that encompasses each peak of interest. The width of the ROIs is determined by the width of the expected peaks of the isotopes of study, which is proportional to the FWHM(E) function:

$$n = n(E) = k \cdot FWHM(E) \tag{3}$$

where k is the proportionality constant to set the desired peak coverage. In this study, the widths of all the ROIs used where set at k = 1.699 for a 95.45% peak area coverage. This selection is meant to maximize the signal-to-noise ratio of a possible artificial isotope with a photopeak in the energy band under monitoring, but what follows is not dependent on the precise coincidence of a photopeak and a ROI. In Fig. 1, an example of the considered ROIs is provided.

3.2. Methodology to obtain the net Regions of Interest

In absence of artificial isotopes, all ROIs centred on a gamma emission of an artificial isotope contain counts from background emission, Compton scattering and possible contributions from tails of the photopeak of natural radionuclides, such as ^{214}Pb, ^{214}Bi and ^{212}Pb. These counts would produce an overestimation in the activity concentration calculation of the artificial isotopes of study if not removed. Therefore, these contributions are subtracted from the ROIs (hereinafter the artificial isotopes ROIs with extra counts will be called *Raw ROIs*) to properly assess the activity concentration of the artificial isotopes (hereinafter the artificial isotopes ROIs with subtracted counts will be called Net ROIs). For a training dataset free from any artificial isotope contribution, we assume each raw ROI to be the sum of four terms, each of them proportional to a ^{222}Rn and ^{220}Rn descendant, plus an independent term accounting for constant contributions present in the environment (presence of ^{40}K, intrinsic background of the detectors or other almost constant natural isotopes).

To determine the values of the coefficients, we produce the training dataset, where we expose our detectors to the natural-emitter source without any artificial sources. We register a set of measurements at different distances between the detector and the source, thus simulating the effect of varying Rn emanations. For each setup, we acquire 10-min spectra and measure the ROIs of ^{212}Pb, ^{214}Pb and ^{214}Bi. Also, we measure the raw ROIs of ^{131}I, ^{137}Cs or ^{60}Co. Since all these measurements are obtained only with presence of natural isotopes (i.e.: ^{238}U descendants, ^{40}K …), we find the parameters that minimize the function *F*:

$$F = \sum_{\forall spec} \left(ROI_{raw}{}^{training} - c_1 \cdot ROI_{214_{Bi}} - c_2 \cdot ROI_{214_{Pb}} - c_3 \cdot ROI_{212_{Pb}} - c_4 \right)^2 \tag{4}$$

We note that this function has only four independent variables, and four parameters to fit. Therefore, even when we have thousands of measurements, the problem is not computationally hard. The result is a set of cleaning parameters (c_1, c_2, c_3, c_4), which is unique for each artificial isotope, each kind of detector and each monitoring site (when applied to on-field monitors). Effectively, the problem is equivalent to solving an overdetermined system of equations for x = (c_1,c_2,c_3,c_4) where for each measurement of ROI_{raw} we also measure the coefficients ROI_{214Bi}, ROI_{214Pb}, ROI_{212Pb}. Therefore, we are obtaining the least-squares minimization of the system $||Ax - ROI_{raw}||^2$, where A is the (3xN) matrix generated by the N measurements of ROI_{214Bi}, ROI_{214Pb}, ROI_{212Pb} and ROI_{raw} is a (1xN) vector. Note that, from this point of view, (c_1, c_2, c_3) quantify the mean spectrum of ROI_{214Bi}, ROI_{214Pb}, and ROI_{212Pb} in the spectral band that corresponds to the gamma emission of the artificial isotope, that we define as ROI_{net} and c_4 is the contribution from a constant background in the same band.

Finally, for a new measurement where artificial isotopes might be present, we can compute the net ROI of each artificial isotope as:

$$ROI_{net} = ROI_{raw} - \left(c_1 \cdot ROI_{214_{Bi}} + c_2 \cdot ROI_{214_{Pb}} + c_3 \cdot ROI_{212_{Pb}} + c_4 \right) \tag{5}$$

3.3. Uncertainty of the net ROIs measurement

Our experimental setup returns the spectral measurements in cps for

each spectral channel. For a given integration time, T_{int}, spent to record the spectrum, the uncertainty of each ROI is derived from Eq. (5) as the sum in quadrature of the uncertainty of ROI_{raw} and the uncertainty of each of the contributions subtracted in the cleaning procedure:

$$\delta ROI_{net} = \sqrt{\delta(ROI_{raw})^2 + \delta(c_1 \cdot ROI_{214_{Bi}})^2 + \delta(c_2 \cdot ROI_{214_{Bi}})^2 + \delta\left(c_3 \cdot ROI_{212_{Pb}}\right)^2 + \delta(c_4)^2} \quad (6)$$

Where uncertainty of each raw ROI can be readily calculated considering that the total number of counts, $ROI_{raw} \cdot T_{int}$ follows Poisson statistics. Therefore,

$$\delta ROI_{raw} = \frac{\delta(ROI_{raw} T_{int})}{T_{int}} = \frac{\sqrt{ROI_{raw} T_{int}}}{T_{int}} = \sqrt{\frac{ROI_{raw}}{T_{int}}} \quad (7)$$

and the uncertainty reduces to:

$$\delta ROI_{net} = \sqrt{\frac{ROI_{raw}}{T_{int}} + \sum_n \left(ROI_n^2 \cdot \delta(c_n)^2 + c_n^2 \cdot \frac{ROI_n}{T_{int}} \right) + \delta(c_4)^2} \quad (8)$$

Where n runs over the ^{214}Bi, ^{214}Pb and ^{212}Pb ROIs. However, there are still terms depending on the uncertainty of the cleaning parameters. To tackle this issue, we generate synthetic datasets reproducing the real dataset, and repeat the minimization procedure many times. This allows us to evaluate the distribution of the parameters c_i. When sampling data to produce synthetic datasets, we must consider that the independent variables related to the emission from natural radioisotopes are strongly correlated among themselves, as they have a common environmental origin. To draw samples that respect this correlation, we follow the Cholesky decomposition method (results for $LaBr_3$(Ce) detector are presented in Appendix I for illustration purposes). This procedure allows us to draw samples from each variable independently, and subsequently correct them to recover the original correlation. Therefore, we generate 100 synthetic datasets from the original fit dataset, and we repeat the minimization procedure, thus obtaining 100 sets of resulting parameters. Finally, we define the uncertainty of each parameter as the range containing 68% of the realizations.

In normal conditions, the net artificial isotopes ROIs fluctuate around 0 cps (note that slightly negative values are possible). The uncertainty fluctuates due to its varying contributions from natural radioisotopes, but it is evaluable for each spectrum. As seen from Eq. (8), the longer the integration time is, the smaller the uncertainty in ROI_{net}.

Prior to the translation of the cps measurements to physical units (activity concentration), we evaluate the detection limit. Following the recommendation by ISO 11929, we first define a decision threshold, ROI_{net}*, as a fixed level of cps that, in absence of a signal, only 5% of the measurements are above the said level. To set the decision threshold we define a dataset with no artificial gamma sources, so that the fluctuations of the net ROIs come exclusively from fluctuations of the background contributions. Once established ROI_{net}*, for each measurement of each ROI, we define the detection limit as the solution to the implicit equation:

$$ROI_{net}{}^{\#} = ROI_{net}{}^{*} + 1.65u(ROI_{net}{}^{\#}) \quad (9)$$

Where, as discussed above, the uncertainty of the measurement u($ROI_{net}{}^{\#}$) is readily available for each measurement, following Eq. (8). In what follows, we consider that an artificial radioisotope is detected if its net ROI is more than its $ROI_{net}^{\#}$. Otherwise, we quote its detection limit, $ROI_{net}^{\#}$. Given the uncertainties of the measurement, $ROI_{net}^{\#}$ shall be understood as the cps that are not exceeded by the true count rate, with a 95% confidence level. For an early warning system, a limit in cps is more robust than one in Bq/m^3, because the conversion to activity concentration units adds uncertainty to the measurement.

3.4. Activity concentration calculation

Finally, we obtain the activity concentration, in Bq/m^3, for the ^{131}I, ^{137}Cs and ^{60}Co. For the artificial isotopes, we assume that the activity concentration (A, in Bq/m^3) is proportional to the net ROI:

$$A = a \cdot ROI_{net} \quad (10)$$

To obtain the calibration coefficient, a, we use point-like sources to produce counts within the considered ROI as if they were produced by the same source homogeneously distributed in air. Fitting the peak of the point-like source to a Gaussian function allows us to obtain the height of the Gaussian, H, and the standard deviation, σ, and we obtain the counts under a peak from the value of $H \cdot \sigma \cdot \sqrt{2\pi}$, which is the integral of the Gaussian function over its entire range. Then, the activity concentration is calculated for each photopeak as:

$$A = \frac{H \cdot \sigma \cdot \sqrt{2\pi}}{\varepsilon \cdot t \cdot p} \quad (11)$$

where ε is the volumetric efficiency obtained using Monte Carlo simulations with isotopes homogeneously distributed in air, t is the counting time and p is the emission probability of the particular gamma-ray being considered.

Next, we can compute a as A divided by ROI_{net} in presence of the source. In this procedure, the only sizeable uncertainty comes from the efficiency factor ε. Following (Korbech and Nielsen, 1992), the maximum relative uncertainty $\delta\varepsilon/\varepsilon$ is less than 3%.

Finally, we are ready to compute the Minimum Detectable Activity Concentration (MDAC). To do so, we propagate the uncertainty due to the calibration factor a, and we solve the equivalent of equation (Casanovas et al., 2016), but this time for $A^{\#}$.

3.5. Activity concentration of natural isotopes

Unlike the artificial isotopes, which in general have activities close to zero, the ROIs of the ^{212}Pb, ^{214}Pb, and ^{214}Bi are dominated by the direct contributions of their actual presence in the environment. In our use case, a fixed place does not guarantee a constant level of natural emissions, but depend on the weather conditions. We simulate these variations in the laboratory by placing at different distances a source of ^{226}Ra with an activity higher than background. To calibrate the natural isotopes in activity concentration, we use a second order equation:

$$A = d_1 \cdot ROI^2 + d_2 \cdot ROI + d_3 \quad (12)$$

Where A is the is the activity concentration, in Bq/m^3, obtained by Gaussian fitting on the natural isotopes peaks, d_i are the calibration coefficients and ROI corresponds to the ROI (raw) obtained for the natural element studied. Placing the sources at different distances from the detectors, we obtain different pairs of A (Bq/m^3)-ROIs values that are fitted to obtain the coefficients d_1, d_2 and d_3 in equation (Cresswell et al., 2006).

3.6. Elements with multiple high-probability emission lines

The application of the method to obtain the activity concentration of ^{60}Co adds a difficulty not found when obtaining ^{137}Cs and ^{131}I activity concentrations. ^{60}Co has two gamma emission lines with a probability close to 100%: 1173 keV (99.97%) and 1332.5 keV (99.98%). To overcome this issue, we apply the method for each emission line individually and then, we calculate the activity concentration as a weighted sum of both activity concentrations.

4. Results

After obtaining the cleaning parameters from the fit dataset, we are ready to apply the algorithm to data taken in presence of artificial isotopes. We have generated a set of scenarios simulating possible situations detected by the Radiological Surveillance Network with different levels of natural emitters, which may occur during varying meteorological conditions (like rainfall events or humidity changes). The measurements were obtained placing the natural source at 40 cm from the $LaBr_3$(Ce) and SrI_2(Eu) detectors (using this source to reproduce a rainfall event), and the ^{131}I, ^{137}Cs and ^{60}Co sources alternatively at 100 cm (we do not perform simultaneous measurements of artificial isotopes). A third setup consists of combinations of each artificial isotope at 100 cm (^{131}I, ^{137}Cs or ^{60}Co) with the natural source at 40 cm. All these scenarios are summarized in Table 1.

All the measurements were realized using the detectors in direct configuration. However, the methodology is also suitable for any other configurations, like particulate filter detectors.

The activity concentration for the natural isotopes results to be for the $LaBr_3$(Ce) detector, in the environmental background scenario, 33.2 $\pm$ 1.4, 35 $\pm$ 3 and 43 $\pm$ 3 Bq/m^3 for ^{212}Pb, ^{214}Pb and ^{214}Bi. In the High Natural Concentration scenario, the corresponding isotopes activity concentrations are 66 $\pm$ 1.6, 271 $\pm$ 5 and 277 $\pm$ 6 Bq/m^3. In the case of the SrI_2(Eu) detector, the environmental background scenario shed 25.0 $\pm$ 0.8, 31 $\pm$ 3 and 38 $\pm$ 3 Bq/m^3 for ^{212}Pb, ^{214}Pb and ^{214}Bi and 44.0 $\pm$ 0.7, 249 $\pm$ 5 and 269 $\pm$ 5 Bq/m^3 in the High Natural Concentration scenario.

4.1. $LaBr_3$(Ce) detector

Fig. 2 shows the activity concentrations calculated using equation (Korbech and Nielsen, 1992) and a Simple Background Subtraction. The latter method relates the counts in the raw ROIs to the activity concentration after applying a Gaussian fitting (which subtracts the intrinsic background and the constant background, being in the case of this article the laboratory background, but not the contributions from natural isotopes to the artificial isotopes ROIs). We examine two scenarios, with and without artificial isotopes. Fig. 3 shows the activity concentrations obtained in the same scenarios applying the cleaning method, subtracting the natural isotopes contributions. The comparation of these two algorithms to calculate the ^{131}I, ^{137}Cs and ^{60}Co activity concentrations is needed due to some research centres apply, or had applied in some point (Baeza et al., 2014), analysis methods with which the results have a similar behaviour to the data showed in Tables 2 and 4 in the Simple Background Subtraction columns. The numerical values for the activity concentrations of each scenario are summarized in Table 2. We also show the MDAC, which varies mainly with the intensity of the natural gamma emitters.

In Table 3, the corresponding MDACs are presented for the 10 min measurements without sources events for 10 min and 24 h measurements calculated using ISO 11929 recommendations. Also, the MDACs values obtained in a previous study using 3σ criteria are presented.

Table 1
Set of measurements with the source of natural isotopes and the different sources of artificial isotopes and distance between detectors and source.

Source	Distance (cm)	Simulated Scenario
Background	–	Environmental Background
Natural	40	High Natural Concentration (HNC)
^{131}I	100	Artificial Isotope Presence
^{137}Cs	100	Artificial Isotope Presence
^{60}Co	100	Artificial Isotope Presence
Natural + ^{131}I	40 + 100	HNC + Artificial Isotope Presence
Natural + ^{137}Cs	40 + 100	HNC + Artificial Isotope Presence
Natural + ^{60}Co	40 + 100	HNC + Artificial Isotope Presence

4.2. SrI_2(Eu) detector

Fig. 4 shows the activity concentrations obtained in the same scenarios as in Figs. 2 and 3 after applying the proposed method for the SrI_2(Eu) detector. The numerical values for the activity concentrations of each event are summarized in Table 4. In Table 5 are presented the corresponding MDAC for the 10 min measurements without sources and 24 h measurements calculated using ISO 11929 recommendations.

Also, the corresponding 10 min MDACs for the ^{131}I, ^{137}Cs and ^{60}Co in the High Natural Concentration scenarios have been calculated, resulting in 6.8/4.2/3.5 Bq/m^3 for an activity concentration of 44 $\pm$ 1, 249 $\pm$ 5 and 269 $\pm$ 5 Bq/m^3 for ^{212}Pb, ^{214}Pb and ^{214}Bi, respectively.

5. Discussion

5.1. Artificial isotopes activity concentrations

The aim of our method is to detect artificial isotopes in the environment. In normal conditions, the amount of such isotopes is null but in case there were actual detections, the presence of natural isotopes would interfere in the activity concentration determination. This situation is clearly present in spectra 45 to 90, in Fig. 2, where the detectors were exposed only to the natural source. The natural isotopes contribute via Compton scattering and peak overlapping with the artificial isotopes ROIs and thus, there is a false positive detection of activity concentrations for the artificial isotopes if no cleaning method is applied. Our method resolves this scenario properly, subtracting all the contributions of the natural isotopes. For example, the activity concentrations of ^{131}I calculated without using our developed method (only the Simple Background Subtraction from raw ROIs are used, see Tables 2 and 4) are 68.4 $\pm$ 2.6 Bq/m^3 for $LaBr_3$(Ce) and 65.6 $\pm$ 2.3Bq/m^3 for SrI_2(Eu), whereas with the proposed method, the activity concentrations are 1.8 $\pm$ 3.4 Bq/m^3 and -2.4 $\pm$ 2.9 Bq/m^3 respectively (Tables 2 and 4), that is, compatible with zero. Therefore, the method is useful to detect and quantify low activity concentrations of artificial isotopes and to avoid false positive detections because the presence of natural isotopes is guaranteed in environmental gamma spectra.

The spectra set 405–450 (Natural + ^{137}Cs), 495–540 (Natural + ^{60}Co), and 585–630 (Natural + ^{131}I) experience the same issue described above with the addition of artificial sources. In all these scenarios, our method subtracts the contributions of natural isotopes leaving only the emission associated to the artificial isotopes. It also returns activity concentration values for the artificial isotopes sources equivalent to the activity concentration values obtained in spectra sets 135–180 (^{137}Cs), 225–270 (^{60}Co) and 315–360 (^{131}I).

As can be observed in Figs. 3 and 4, the results for ^{131}I show slightly more dispersion than those for ^{137}Cs and ^{60}Co (spectra sets 45–90, 405–450 and 495–540). This is expected, as the ^{131}I ROI overlaps partially with the 364 keV photopeak from ^{214}Pb and there are also contributions from Compton scattering. Therefore, the fluctuations of the ^{214}Pb ROI produce large relative variations of the ^{131}I ROI, which in absence of a ^{131}I source is about 0. The opposite is also true: in case that ^{131}I is present, the ^{214}Pb ROI and its fluctuations increase. Consequently, the uncertainty associated with the ^{131}I net ROI also increases, which translates to an increase in MDAC. This poses a paradox: it seems a priori possible that adding a ^{131}I source increases the difficulty to detect it. To

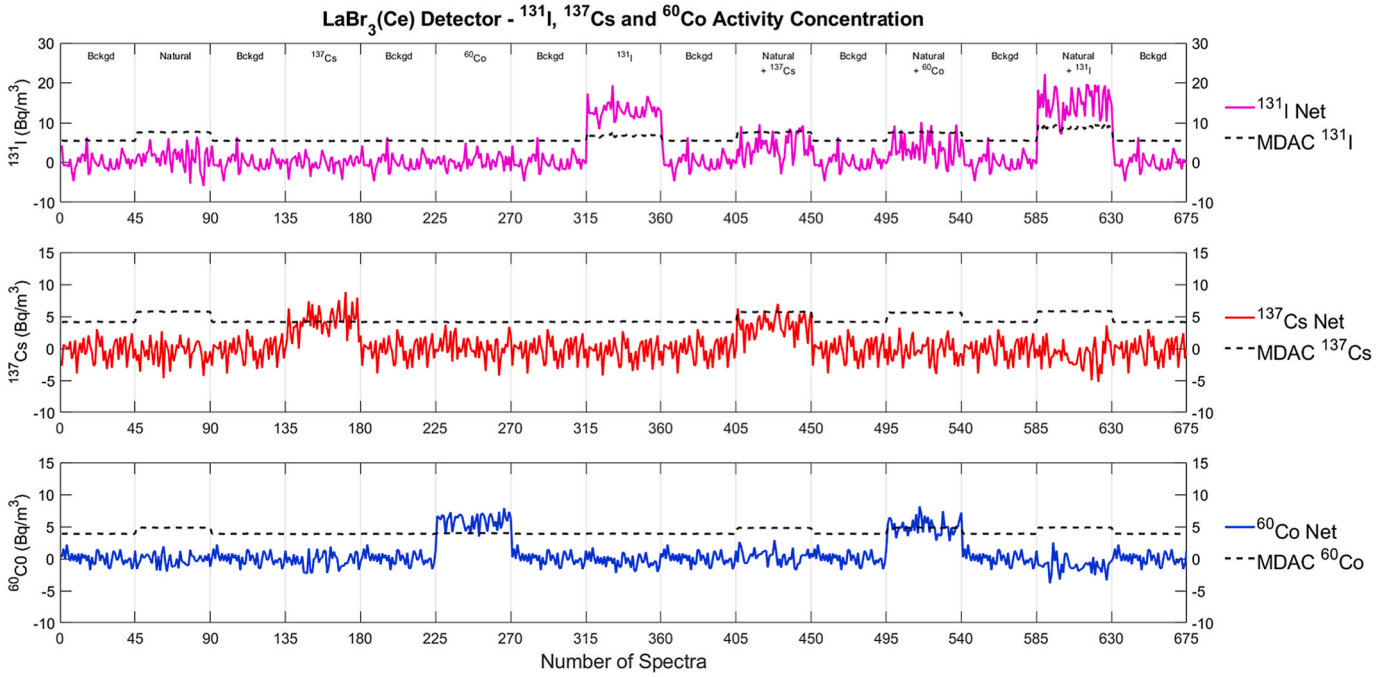

Fig. 3. Net data for the $LaBr_3$(Ce) detector with scenarios with natural, ^{131}I, ^{137}Cs and ^{60}Co isotopes sources. The scenarios are the same than in Fig. 2. The dashed line indicates the MDAC. Note that only when the corresponding source is present, the net ROIs are systematically above the MDAC.

Table 2
Activity concentration values for the respective artificial isotope in each one of the situations studied applying the proposed method (results in Fig. 3) or the Simple Background Subtraction (from raw ROIs) (results in Fig. 2) in a $LaBr_3$(Ce).

Scenario	Proposed Method (from ROI_{net}) (Bq/m^3)			Simple Background Subtraction (from ROI_{raw}) (Bq/m^3)		
	^{131}I	^{137}Cs	^{60}Co	^{131}I	^{137}Cs	^{60}Co
Natural	1.8 ± 3.4	−0.6 ± 1.8	−0.2 ± 1.1	68.4 ± 2.6	15.4 ± 1.8	8.0 ± 0.8
^{131}I	12.8 ± 1.8	−0.4 ± 1.6	−0.5 ± 0.9	13.1 ± 1.5	0.2 ± 1.6	0.00 ± 0.7
^{137}Cs	−0.2 ± 1.8	4.2 ± 2.0	−0.3 ± 1.1	−1.2 ± 1.5	3.9 ± 2.1	−0.4 ± 0.9
^{60}Co	0.2 ± 1.6	0.3 ± 1.8	5.9 ± 1.1	−0.5 ± 1.2	0.1 ± 1.8	5.0 ± 0.9
Natural + ^{131}I	16.3 ± 3.5	−1.3 ± 1.8	−1.0 ± 1.1	82.4 ± 2.7	14.8 ± 1.8	6.9 ± 0.9
Natural + ^{137}Cs	4.9 ± 3.1	4.0 ± 1.6	0.3 ± 1.2	66.7 ± 2.4	19.2 ± 1.6	8.0 ± 1.0
Natural + ^{60}Co	3.4 ± 3.2	−0.3 ± 1.7	5.1 ± 1.3	63.9 ± 2.4	14.2 ± 1.7	11.8 ± 1.0
Background	−0.2 ± 1.8	−0.04 ± 1.6	−0.03 ± 0.9	0.00 ± 1.5	−0.1 ± 1.6	0.00 ± 0.7

explore this possibility, we move the ^{131}I source away from the detector, thus simulating three fainting ^{131}I activity concentrations (Fig. 5). The result is that very close to the basis MDAC (that is, the MDAC in absence of ^{131}I source) it is possible to have false negatives due to downwards fluctuations in the ^{131}I ROI. However, the ^{131}I MDAC increases very slowly as the true ^{131}I activity concentration grows, which means that this drawback is only relevant for a very narrow range of activities very close to the basis MDAC.

Slight differences in ^{131}I activity concentration obtained for the spectra sets 315–360 (^{131}I scenario) in $LaBr_3$(Ce) and SrI_2(Eu) detectors are fully compatible taking into account the corresponding measurement error (12.8 ± 1.8 Bq/m^3 vs 15.4 ± 1.5 Bq/m^3). However, some variation is expected due to differences in the radioactive source positioning from one detector to another.

When obtaining the ambient equivalent dose H*(10)- from spectra (Casanovas et al., 2016), calculations show values between 0.28 (for ^{137}Cs) and 2.5 nSv/h (for ^{60}Co) above the laboratory background of 120 ± 2 nSv/h (mean value and 3σ) when we place the artificial isotopes sources. Very low activity concentration increments in spectra do not show a remarkable increase in ambient equivalent dose values (between 0.2% and 2% increase from background value). However, our method can discern a positive detection of an artificial isotope and obtaining its activity concentration. These results show the importance of using gamma spectrometry with analysis methods for early warning.

5.2. MDAC

The MDAC of each net ROI depends on the contribution of the natural isotopes in the studied spectral band. Therefore, we cannot attribute a single value for the MDAC of our equipment and analysis method. Instead, we have a variable MDAC for each spectrum, which vary mainly

Table 3
MDAC obtained for ^{131}I, ^{137}Cs and ^{60}Co after application of the proposed method for each scenario for the $LaBr_3$(Ce) detector for 10 min measurements without sources (dashed lines in Figs. 3) and 24h measurements without sources.

Isotope	MDAC 10 min from this study (Bq/m^3)	MDAC 10 min from previous study (Prieto et al., 2018b) (Bq/m^3)	MDAC 24 h from this study (Bq/m^3)
^{131}I	5.4	5.7	3.4
^{137}Cs	4.1	4.3	2.9
^{60}Co	3.9	–	1.7

Also, the corresponding 10 min MDACs for the ^{131}I, ^{137}Cs and ^{60}Co in the High Natural Concentration scenarios have been calculated, resulting 7.6/5.8/4.8 Bq/m^3 for an activity concentration of 66 ± 2, 271 ± 5 and 277 ± 6 Bq/m^3 for ^{212}Pb, ^{214}Pb and ^{214}Bi, respectively.

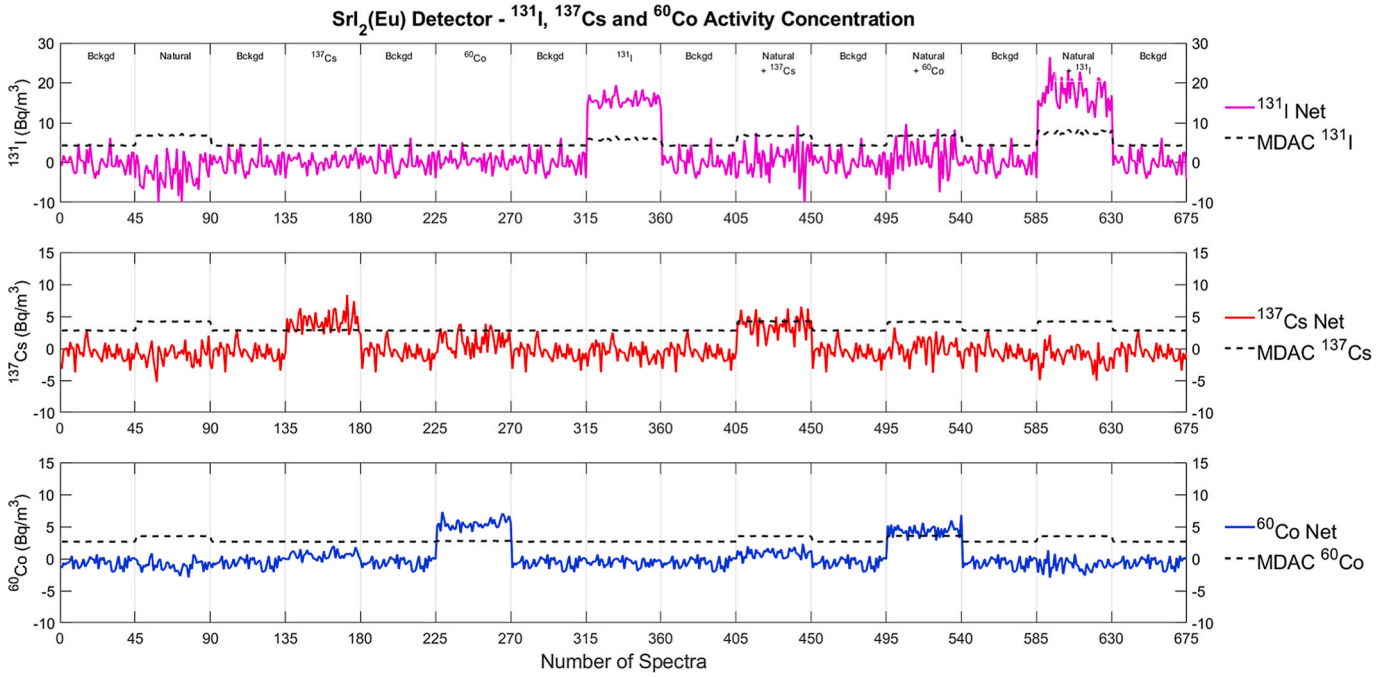

Fig. 4. Net data for the $SrI_2(Eu)$ detector with events with natural, ^{131}I, ^{137}Cs and ^{60}Co isotopes sources. The scenarios are the same than in Figs. 2 and 3. The dashed line indicates the MDAC. Note that only when the corresponding source is present, the net ROIs are systematically above the MDAC.

Table 4
Activity concentration values for the respective artificial isotope in each one of the situations studied applying the proposed method (results in Fig. 4) or the Simple Background Subtraction in a $SrI_2(Eu)$.

Scenario	Proposed Method (from ROI_{net}) (Bq/m^3)			Simple Background Subtraction (from ROI_{raw}) (Bq/m^3)		
	^{131}I	^{137}Cs	^{60}Co	^{131}I	^{137}Cs	^{60}Co
Natural	−2.4 ± 2.9	−1.1 ± 1.5	−0.8 ± 0.9	65.6 ± 2.3	11.5 ± 1.3	9.4 ± 0.7
^{131}I	15.4 ± 1.5	−0.5 ± 1.3	−0.6 ± 0.7	15.2 ± 1.2	0.4 ± 1.1	0.00 ± 0.5
^{137}Cs	0.5 ± 1.6	4.1 ± 1.5	0.5 ± 0.6	−0.9 ± 1.2	3.6 ± 1.4	0.2 ± 0.5
^{60}Co	0.5 ± 1.5	1.0 ± 1.4	5.4 ± 0.7	−0.9 ± 1.2	0.8 ± 1.3	4.2 ± 0.6
Natural + ^{131}I	16.9 ± 4.1	−1.1 ± 1.6	−0.8 ± 0.9	87.3 ± 3.0	16.5 ± 1.4	10.3 ± 0.7
Natural + ^{137}Cs	1.2 ± 5.0	4.0 ± 1.6	0.9 ± 0.8	66.3 ± 3.8	19.4 ± 1.5	10.5 ± 0.6
Natural + ^{60}Co	1.5 ± 3.9	0.1 ± 1.5	4.4 ± 0.8	66.3 ± 3.0	15.6 ± 1.4	13.2 ± 0.7
Background	0.1 ± 1.5	−0.2 ± 1.3	0.01 ± 0.7	0.00 ± 1.2	0.00 ± 1.1	0.00 ± 0.5

Table 5
MDAC obtained for ^{131}I, ^{137}Cs and ^{60}Co after application of the proposed method for each scenario for the $SrI_2(Eu)$ detector for 10 min measurements without sources (dashed lines in Figs. 4) and 24h measurements without sources.

Isotope	MDAC 10 min from this study (Bq/m^3)	MDAC 24 h from this study (Bq/m^3)
^{131}I	4.2	2.1
^{137}Cs	2.8	1.7
^{60}Co	2.7	1.2

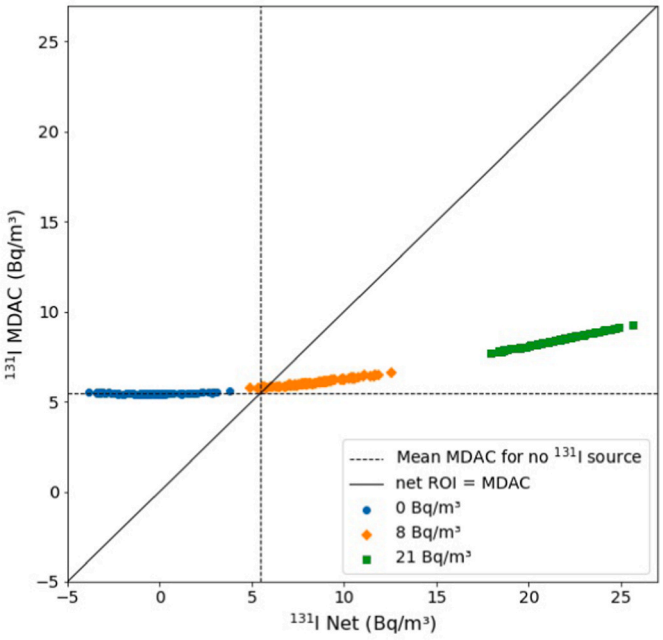

Fig. 5. Dependency of the ^{131}I MDAC with the ^{131}I activity concentration itself, as measured in 10-min exposures with the $LaBr_3(Ce)$ detector. The plot shows the fluctuation of the measured activity concentration for no source, a concentration of 8 Bq/m^3, and a concentration of 21 Bq/m^3 homogeneously distributed in air. The diagonal line separates detections (bottom-right) from non-detections (upper-left). The dashed line is the mean of the MDACs in absence of source (5.4 Bq/m^3 as shown in the Table 3) and is also placed vertically. Very few measurements lay right of the vertical line and left of the diagonal line. These are false negatives despite having activity concentration above the MDAC for no source.

as the result of the variations in the emission of ^{214}Bi, ^{214}Pb and ^{212}Pb. The best-case scenario is that where these natural emissions are minimal. The introduction of radon-descendant sources in the vicinity of the detector are thus seen as steps in the MDAC, which may make the artificial isotope detection more difficult even if the emission of the artificial isotope remains constant. In case of field detectors, where the variations

of natural emitters are not sudden, but vary smoothly as a result of the meteorological conditions, also the MDAC curve is expected to vary smoothly.

Regardless of the intensity of the natural emitter, the MDAC for ^{131}I is always the highest, and the one that grows faster as ^{214}Pb emission increases. This is because of the overlap of the ^{131}I ROI with the ^{214}Pb photopeak in both $LaBr_3$(Ce) and SrI_2(Eu) detector types. Moreover, gammas from Compton dispersion concentrate in the area of lower energies of the spectra, where the 364 keV ^{131}I gamma emission is. In contrast, MDAC for ^{60}Co is lower: gammas from ^{60}Co have a higher energy (1173 keV and 1332.5 keV) and can be found in an area where the influence of natural emissions and their associated interaction mechanisms is less predominant.

The MDAC values obtained for ^{131}I, ^{137}Cs or ^{60}Co for 10 min spectra in $LaBr_3$(Ce) in background scenarios are comparable with the values obtained in (Prieto et al., 2018b) and the discrimination criteria discussed there. Also, if we compare the MDAC values obtained with the $LaBr_3$(Ce) and SrI_2(Eu) detectors, it follows that the MDAC is lower for the SrI_2(Eu) detector as expected, due to the fact the SrI_2(Eu) does not have self-contamination (intrinsic background).

The *Natural* + ^{137}*Cs* scenario deserves special attention. In both detectors our method returns an activity concentration value similar or lower than the corresponding MDAC. This situation arises as a result of 1) The ^{137}Cs activity is slightly higher than the MDAC in the scenario when only the ^{137}Cs source is placed and 2) The MDAC increases due to the presence of the natural isotopes. In fact, this result is a good new: even in such bad situation, our method returns a consistent value for both detectors.

5.3. Applicability of the method to other conditions

As explained in the *Methods* section, our method needs different natural isotopes activity concentrations as input data. These data are used to obtain the coefficients that allow to subtract the natural isotopes contributions to the raw ROIs and to determine the activity concentrations of the isotopes of interest correctly.

Implementing the method in monitoring network stations strongly depends on the natural isotopes of the station location. Thus, to obtain the cleaning equations for each monitoring site we need to acquire a reasonable amount of environmental data containing different levels of activity concentrations of ^{212}Pb, ^{214}Pb and ^{214}Bi. These data are obtained during periods with and without rainfall events. Also, these data are used to calibrate in Bq/m^3 the natural occurring isotopes, obtaining from them the activity concentration by Gaussian fitting in the spectrum and the values of the ROIs and fitting the results to obtain equation (Cresswell et al., 2006) coefficients.

The activity concentrations of the scenarios tagged as *Background*, showed in Fig. 2, are more realistic than the scenarios with high concentration of natural isotopes (HNC) which reproduce an extreme situation. Consider that the highest activity concentration of the natural isotopes ever registered by the Radiological Surveillance Network of Catalonia is lower than 150 Bq/m^3. Consequently, in habitual conditions the method resolves correctly and experiences less dispersion in ^{131}I results.

In the event of simultaneous detection of ^{131}I, ^{137}Cs and ^{60}Co or detection of different artificial isotopes not considered in this study, as for instance during a nuclear accident (IAEA. The Fukushima Daiichi Accident, 2015), there could be an increase of counts in the ^{131}I, ^{137}Cs and ^{60}Co ROIs. In such case, the method would not perfectly quantify the activity concentration of the artificial isotopes. Therefore, a positive signal in the ^{131}I, ^{137}Cs or ^{60}Co ROIs does not unambiguously guarantee that ^{131}I, ^{137}Cs or ^{60}Co have been detected. But it does mean that a robust alert is to be issued, and the corresponding spectrum must be further analysed. In particular, this effect is shown in Figs. 3 and 4 where the presence of ^{137}Cs and ^{60}Co (spectra 405–450 and 495–540) causes an increment in ^{131}I ROI, with sporadic surpassing of MDAC values in some measurements.

6. Conclusions

We have developed a method that detects and quantifies artificial isotopes, removing the possible natural variable contributions and the constant background in real time environmental gamma spectrometry measurements.

The model presents the great advantage of being independent from the technology used to detect the radioisotopes, using the same procedure to obtain the cleaning algorithm for $LaBr_3$(Ce) or SrI_2(Eu). As a result, all the artificial isotopes activity concentration values are consistent for all the scenarios and for both detectors. Note that the proportionality coefficients obtained with equation (Prieto et al., 2018a) are assumed to remain constant for each monitor as long as the monitor characteristics, such as location or multichannel analyser parameters, are not modified.

While ^{131}I, ^{137}Cs and ^{60}Co are the main gamma indicators of a problem in a nuclear facility and deserve special attention, we can define other regions in the spectrum for dedicated monitoring in case specific circumstances make this advisable.

The method is conceptually very simple, easy to implement and extremely effective in monitoring automatically the regions of the spectrum that correspond to gamma emissions from radionuclides such as ^{131}I, ^{137}Cs and ^{60}Co. Moreover, the computing power to run our method is negligible, making it very advisable for automated monitoring networks and early warning.

Authorship contributions

Conception and design of study: **M. Salvadó, A. Cerezo, I. Reichard, E. Prieto**; acquisition of data: **A. Cerezo**; analysis and/or interpretation of data: **A. Cerezo, I. Reichard, M. Salvadó, R. Casanovas, E. Prieto.**

Drafting the manuscript: **A. Cerezo, I. Reichard, E. Prieto, M. Salvadó, R. Casanovas**; revising the manuscript critically for important intellectual content: **A. Cerezo, I. Reichard, E. Prieto, M. Salvadó, R. Casanovas.**

Approval of the version of the manuscript to be published (the names of all authors must be listed): **A. Cerezo, E. Prieto, I. Reichard, R. Casanovas, M. Salvadó.**

Declaration of competing interest

The authors declare that they have no known competing financial interests or personal relationships that could have appeared to influence the work reported in this paper.

Data availability

Data will be made available on request.

Acknowledgements

All persons who have made substantial contributions to the work reported in the manuscript (e.g., technical help, writing and editing assistance, general support), but who do not meet the criteria for authorship, are named in the Acknowledgements and have given us their written permission to be named. If we have not included an Acknowledgements, then that indicates that we have not received substantial contributions from non-authors.

Appendix I. use of the Cholesky decomposition method to generate synthetic datasets

In Section 3 we need to extract random values of ROI. In practice, for each of these ROIs we generate a vector with the repeated measurements. These values have strong linear correlations among themselves for two reasons (Fig A1): i) the causes for increased natural radioactivity are the same regardless of the emitter (meteorological causes for field detectors, or varying distance of the source for lab measurements); and ii) some natural emitters belong to the same disintegration chain, particularly ^{214}Bi and ^{214}Pb.

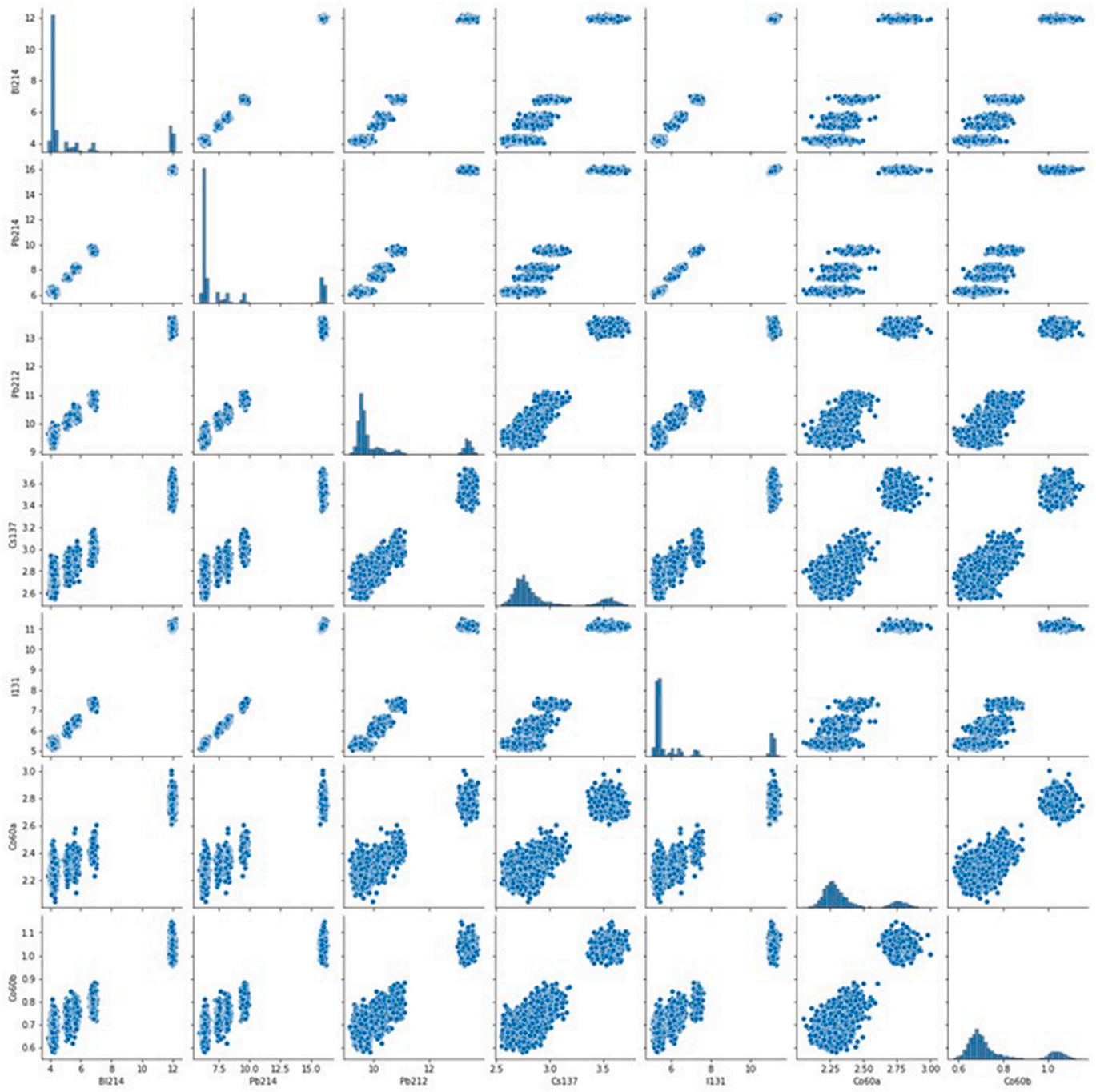

Fig. A1. Fit dataset for the $LaBr_3$(Ce) detector with varying source of ^{214}Bi, ^{214}Pb and ^{212}Pb. Diagonal panels: distribution of values of each ROI; non-diagonal panels: scatter plot for each ROI as a function of the others.

After several spectral measurements, we can randomly draw values from each vector. However, there is no guarantee that say, a high measurement of ^{214}Bi will be drawn along a correspondingly high measurement of ^{137}Cs. For this reason, we first produce the Cholesky decomposition matrix, which is itself derived from the correlation coefficients matrix of the variables. Then, for each ROI, we fill the columns of an uncorrelated matrix by randomly sampling that ROI from the original dataset. Finally, the synthetic dataset with the restored correlations is the matrixial product of the uncorrelated matrix by the Cholesky matrix. With these synthetic datasets we repeat the minimization procedure and reconstruct the distribution of values of each parameter (Fig A2). Finally, given the distributions, we estimate the range of each parameter containing the 68% of the realizations, which we take as the uncertainty in the said parameter.

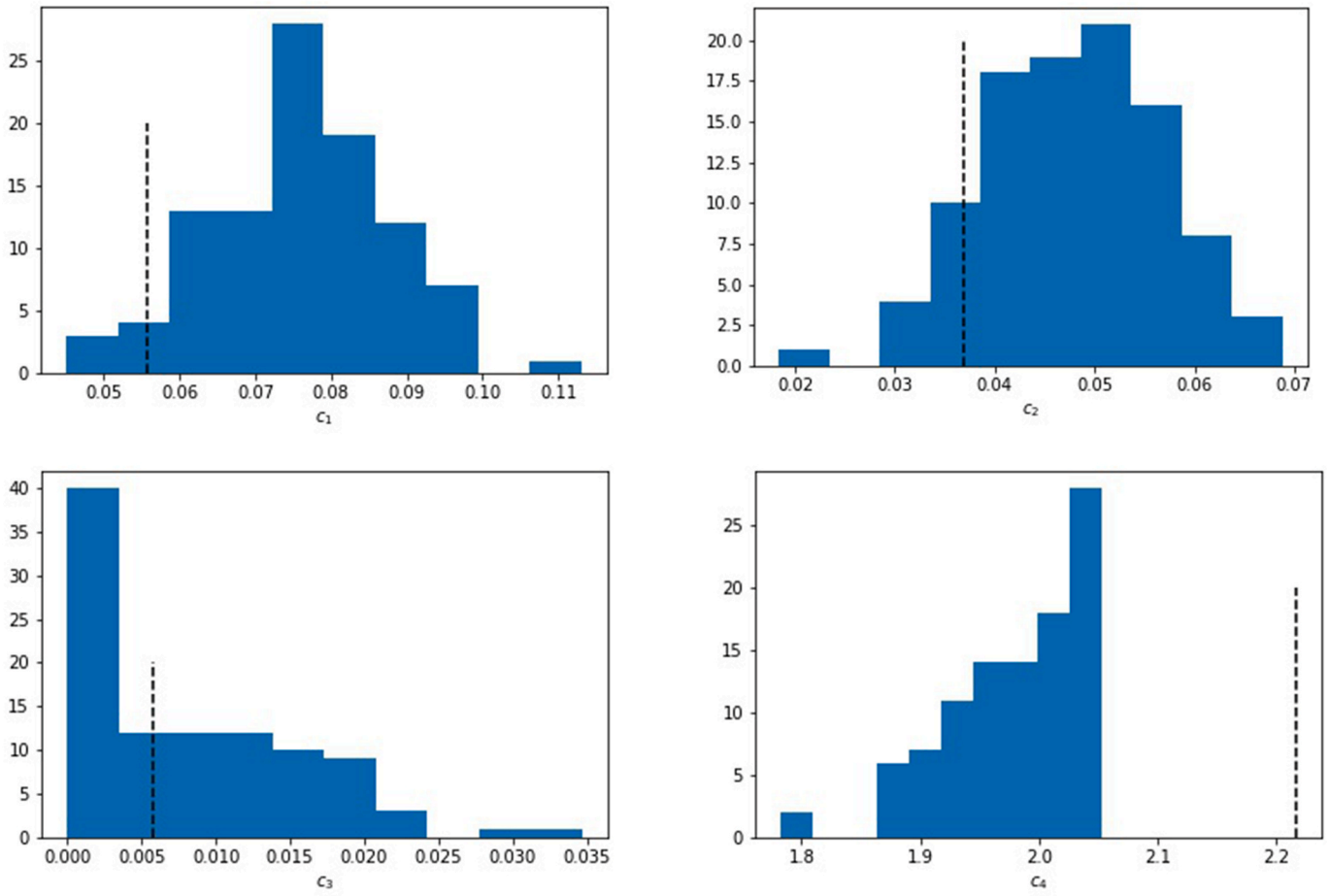

Fig. A2. Distributions of the cleaning parameters (c_1, c_2, c_3, c_4) for the ^{137}Cs ROI with 100 synthetic datasets. The value for the original dataset is indicated as a dashed vertical line.

Appendix II. Energy, resolution and efficiency calibration curves for $LaBr_3(Ce)$ and $SrI_2(Eu)$ detectors

In the following 3 figures, we present the energy, resolution or FWHM(E) and efficiency calibration curves for the $LaBr_3(Ce)$ and $SrI_2(Eu)$ detectors used in this study. The general formula, coefficients and R^2 are included in each case. To obtain these results, the same methodologies as those described in previous studies have been used (Casanovas et al., 2012c; Hurtado et al., 2004).

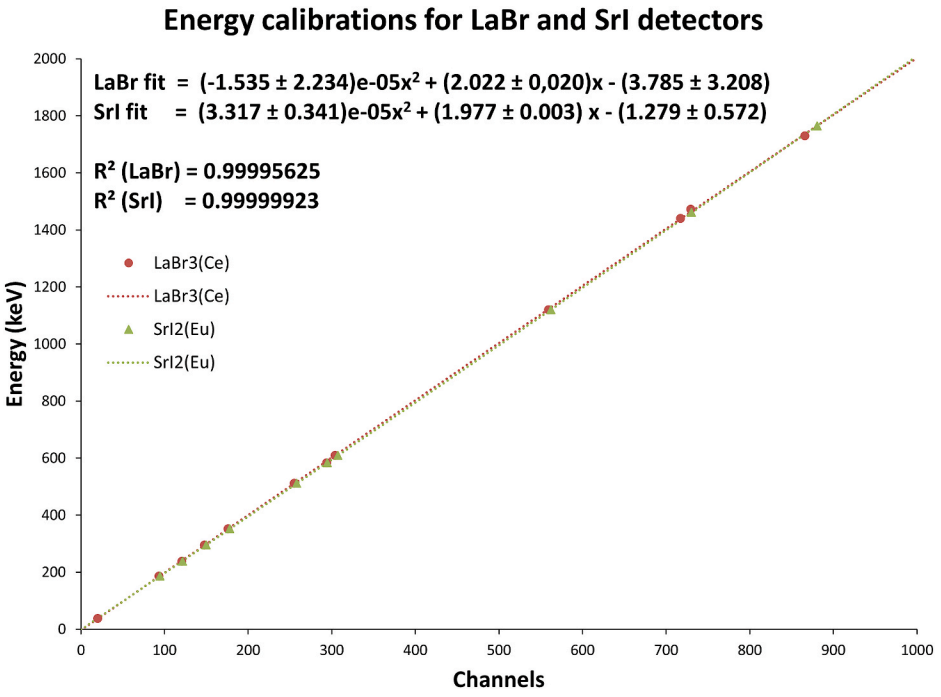

Fig. A3. Energy calibration for $LaBr_3(Ce)$ and $SrI_2(Eu)$ detectors. The dots indicate the measurements made and the dashed line the fitting to the experimental values. In the upper part are shown the fitting parameters.

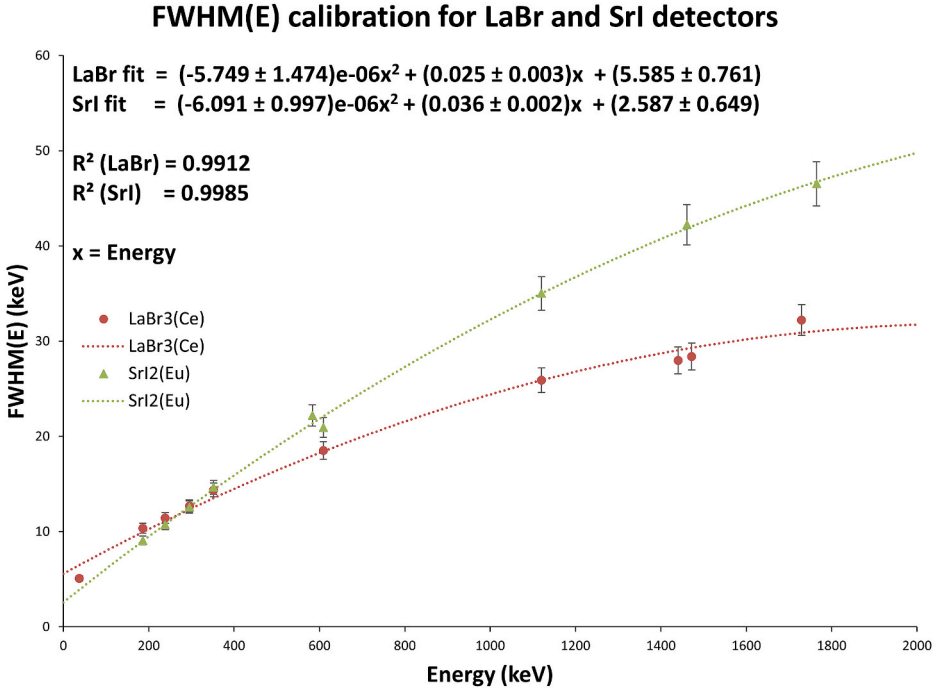

Fig. A4. Resolution calibration for $LaBr_3(Ce)$ and $SrI_2(Eu)$ detectors. The dots indicate the measurements made and the dashed line the fitting to the experimental values to obtain the FWHM€. In the upper part are shown the fitting parameters.

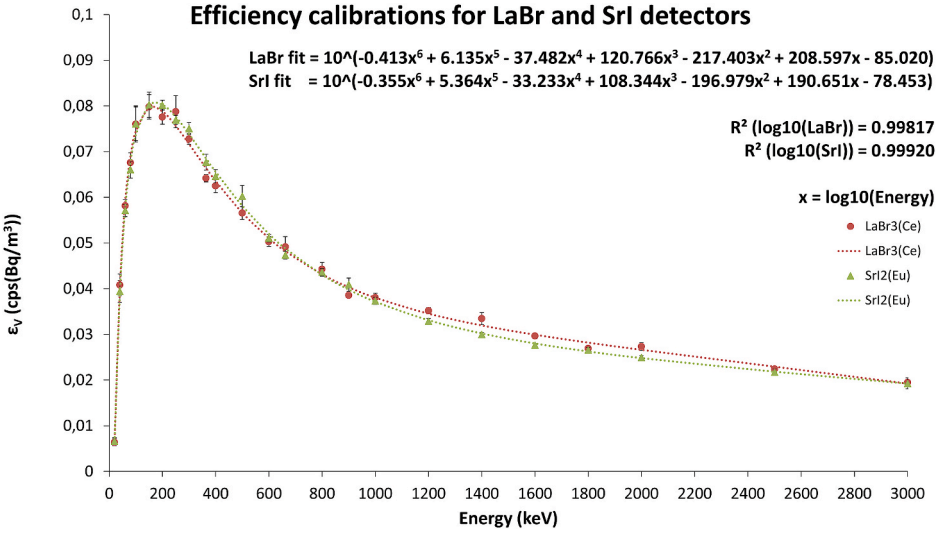

Fig. A5. Efficiency calibration for $LaBr_3(Ce)$ and $SrI_2(Eu)$ detectors. The dots indicate the measurements made and the dashed line the fitting to the experimental values to obtain the efficiency (m^3). In the upper part are shown the fitting parameters. The differences in efficiency error are due to the variance reduction method used in the Monte Carlo simulation, called Direction Bias Method (DBM).

References

Androulakaki, E.G., Kokkoris, M., Tsabaris, C., Eleftheriou, G., Patiris, D.L., Pappa, F.K., et al., 2016. In Situ γ-ray Spectrometry in the Marine Environment Using Full Spectrum Analysis for Natural Radionuclides [cited 2023 Jan 23]; Available from. https://doi.org/10.1016/j.apradiso.2016.05.008.

Baeza, A., Caballero, J.M., JÁ, Corbacho, Ontalba Salamanca, M.Á., Vasco, J., 2014. Proposed improvements to existing water monitoring systems in automatic radiological warning networks. J. Radiol. Prot. 34 (2), 313–324.

Baeza, A., Rodríguez-Perulero, A., Guillén, J., 2016. Anthropogenic and naturally occurring radionuclide content in near surface air in Cáceres (Spain). J. Environ. Radioact. 165 (September 2004), 24–31.

Casanovas, R., Morant, J.J., López, M., Hernández-Girón, I., Batalla, E., Salvadó, M., 2011. Performance of data acceptance criteria over 50 months from an automatic real-time environmental radiation surveillance network. J. Environ. Radioact. 102 (8), 742–748.

Casanovas, R., Morant, J.J., Salvadó, M., 2012a. Temperature peak-shift correction methods for NaI(Tl) and LaBr 3(Ce) gamma-ray spectrum stabilisation. Radiat. Meas. 47 (8), 588–595.

Casanovas, R., Morant, J.J., Salvadó, M., 2012b. Energy and resolution calibration of NaI (Tl) and LaBr 3(Ce) scintillators and validation of an EGS5 Monte Carlo user code for efficiency calculations. Nucl. Instrum. Methods Phys. Res. 675, 78–83.

Casanovas, R., Morant, J.J., Salvadó, M., 2012c. Energy and resolution calibration of NaI (Tl) and LaBr 3(Ce) scintillators and validation of an EGS5 Monte Carlo user code for efficiency calculations. Nucl. Instrum. Methods Phys. Res. 675, 78–83.

Casanovas, R., Morant, J.J., Salvadó, M., 2013. Implementation of gamma-ray spectrometry in two real-time water monitors using NaI(Tl) scintillation detectors. Appl. Radiat. Isot. 80, 49–55.

Casanovas, R., Morant, J.J., Salvado, M., 2014a. Development and calibration of a real-time airborne radioactivity monitor using gamma-ray spectrometry on a particulate filter. IEEE Trans. Nucl. Sci. 61 (2), 727–731.

Casanovas, R., Morant, J.J., Salvadó, M., 2014b. Development and calibration of a real-time airborne radioactivity monitor using direct gamma-ray spectrometry with two scintillation detectors. Appl. Radiat. Isot. 89, 102–108.

Casanovas, R., Prieto, E., Salvadó, M., 2016. Calculation of the ambient dose equivalent H*(10) from gamma-ray spectra obtained with scintillation detectors. Appl. Radiat. Isot. 118.

Cresswell, A.J., Sanderson, D.C.W., White, D.C., 2006. 137Cs measurement uncertainties and detection limits for airborne gamma spectrometry (AGS) data analysed using a spectral windows method. Appl. Radiat. Isot. 64 (2), 247–253.

Hendriks, P.H.G.M., Limburg, J., de Meijer, R.J., 2001. Full-spectrum analysis of natural g-ray spectra. J. Environ. Radioact. 53, 365–380.

Hötzl, H., Winkler, R., 1987. Activity concentrations of 226Ra, 228Ra, 210Pb, 40K and 7Be and their temporal variations in surface air. J. Environ. Radioact. 5, 445–458, 1987;5:1–2.

Hurtado, S., Garc, M., Ia-Le, Garc! Ia-Tenorio, R., 2004. GEANT4 code for simulation of a germanium gamma-ray detector and its application to efficiency calibration. Nucl. Instrum. Methods Phys. Res. 518, 764–774.

IAEA. The fukushima Daiichi accident: radiological consequences. Fukushima Daiichi Accid. 4/5, 2015, 4:237.

International Atomic Energy Agency, 1999. Generic Procedures for Monitoring during a Nuclear or Radiological Emergency. Public Health.

ISO 11929-1, 2019. Determination of the Characteristic Limits (Decision Threshold, Detection Limit and Limits of the Coverage Interval) for Measurements of Ionizing Radiation — Fundamentals and Application — Part 1: Elementary Applications.

Korbech, U., Nielsen, K.G., 1992. A simple method for early detection of fall-out. Radiat. Protect. Dosim. 40 (2), 103–109.

Márquez, J.L., Benito, G., Saez, J.C., Navarro, N., Alvarez, A., Quiñones, J., 2017. The influence of radon (gas and progeny) and weather conditions on ambient dose equivalent rate. Radiat. Protect. Dosim. 174 (3), 423–430.

Prieto, E., Casanovas, R., Salvadó, M., 2018a. Calibration and performance of a real-time gamma-ray spectrometry water monitor using a LaBr3(Ce) detector. Radiat. Phys. Chem. 144 (September 2017), 444–450.

Prieto, E., Casanovas, R., Salvadó, M., 2018b. Spectral windows analysis method for monitoring anthropogenic radionuclides in real-time environmental gamma-ray scintillation spectrometry. J. Radiol. Prot. 38 (1), 229–246.

Vallés, I., Camacho, A., Ortega, X., Serrano, I., Blázquez, S., Pérez, S., 2009. Natural and anthropogenic radionuclides in airborne particulate samples collected in Barcelona (Spain). J. Environ. Radioact. 100 (2), 102–107.